J. Fluid Mech. (1975), *vol.* 70, *part* 2, *pp.* 369–392
Printed in Great Britain

Laser-Doppler anemometer measurements in drag-reducing channel flows

By M. M. REISCHMAN† AND W. G. TIEDERMAN

School of Mechanical and Aerospace Engineering,
Oklahoma State University, Stillwater

(Received 2 July 1974 and in revised form 8 November 1974)

The objective of this study was to make velocity measurements in drag-reducing flows which would be sufficient in scope and accuracy to test proposed models of drag-reducing flows and to yield new information about the mechanisms of drag reduction. Consequently, measurements of the mean and turbulence intensity of the streamwise velocity component were made in fully developed, turbulent, drag-reducing flow in a two-dimensional channel with a laser-Doppler anemometer. The anemometer was operated in the individual-realization mode and corrections were made to eliminate statistical biasing of the data. Two polyacrylamides and a polyethylene oxide were used to produce seven flows which had drag reductions ranging from 24 to 41 %. Measurements were also made in water to establish the standard characteristics of the flow channel.

The data show that the drag-reducing mean velocity profile can be divided into three zones: a viscous sublayer, a buffer or interactive region and a logarithmic region. There is no evidence that the viscous sublayers of the drag-reducing channel flows are thicker than those in the solvent flows. In addition the normalized streamwise fluctuations are essentially the same in both the solvent and drag-reducing sublayers. The changes caused by the polymer addition occur in the buffer region. The drag-reducing buffer region is thicker and the velocity profile in the outer flow region adjusts in order to accommodate this buffer-region thickening. The measurements of the streamwise velocity fluctuations also show that the polymer additives redistribute the primary turbulent activity over a broadened buffer region. The normalized magnitude of these fluctuations is, however, considerably lower in these two-dimensional drag-reducing channel flows than in those previously reported by Rudd (1972), Logan (1972) and Kumor & Sylvester (1973). Moreover, the mean velocity profiles in the buffer region do not confirm the hypothesis of Virk, Mickley & Smith (1970) that the data will follow their proposed 'ultimate profile' when the drag reduction is less than that given by the maximum asymptote. The mean velocity measurements also show that the proposed methods for predicting the upward shift in the outer portion of the mean velocity profile are inconsistent and lack universality. However, these results do confirm the previous suggestions of Virk (1971), Tomita (1970) and Lumley (1973) that the buffer region is the area of importance and change in drag-reducing flows.

† Present address: Naval Undersea Center, San Diego, California.

1. Introduction

The general characteristics of drag reduction can best be understood in terms of the definition offered by Lumley (1969). He defined drag reduction as the "reduction of skin friction in turbulent flow below that of the solvent alone". The "reduction of skin friction" refers to the lowering of the wall shearing stress when small amounts of a long-chain polymer are added to a Newtonian solvent to form a thermodynamically dilute solution. As the definition points out, the addition of polymer results in drag reduction only when the flow is turbulent.

Drag reduction has been studied by various techniques. Pressure drop–flow rate experiments have shown the magnitude and scope of the phenomenon. Flow-visualization experiments have given some insight into the drag-reduction mechanism and have provided the basis for qualitative interpretations of various aspects of drag-reducing flow. Numerous velocity measurements have been made in an attempt to quantify the effect of polymer additives. Unfortunately these previous experiments have not yielded conclusive results because either an ambiguous measurement technique was used or the measurements were made in a poorly understood flow field. Consequently the results have been difficult to interpret and lack general engineering applicability.

The purpose of the experimental measurements reported here was to measure accurately the mean and fluctuating velocities of a drag-reducing, fully developed, two-dimensional, turbulent channel flow. The intention was to make velocity measurements representative of a broad range of drag-reducing flows, and to use the measurements to test hypotheses and prediction techniques for drag-reducing velocity profiles and to make inferences about the drag-reduction mechanism.

Inherent within this purpose was the fundamental desire to measure accurately the effects of polymer additives on only turbulent processes. Consequently, a two-dimensional channel flow was selected because this is a well-understood Newtonian flow which possesses all the essential features of shear-flow turbulence; namely production, convection and dissipation. Similarly a laser anemometer measuring individual realizations (LAMIR) was selected as the anemometer because it will yield accurate measurements in the high-fluctuation near-wall region of dilute polymer flows. This technique also has the advantages of straightforward and unambiguous data analysis. Good spatial resolution was achieved by slightly bowing the side walls of the channel and aligning the laser beams parallel to these walls. Velocity measurements were made in solvent flows and in flows of dilute polymer solutions where systematic variations in the polymer type and flow rate were made. Both polyethylene oxide and polyacrylamide molecules were used, giving a molecular weight range of 4×10^6 to 15×10^6.† The drag-reducing flow rates were varied, yielding shear velocities varying from 0·019 to 0·040 m/s and friction reductions ranging from 24 to 41 %. The Reynolds number based on mass-average velocity, hydraulic diameter and solvent viscosity varied from 20 200 to 52 400. The sample sizes of the indi-

† Advertised weight-averaged molecular weights.

vidual velocity realizations were large enough to ensure (at the 95 % confidence interval) that all the mean velocity measurements had uncertainties of less than 5 % while the bulk of the mean estimates had uncertainties less than 3 %.

The inconclusiveness of past velocity measurements in drag-reducing flows is exemplified by the 20 or more major experiments conducted to date. These experiments, which were reviewed by Reischman (1973), can be subdivided according to measurement techniques, that is bubble tracing, laser-Doppler anemometers, hot-element probes and Pitot probes. The extensive difficulties and errors associated with using either Pitot probes or hot-element probes in dilute polymer solutions are well known and well summarized by Hoyt (1972). Bubble tracing is an extremely tedious process, consequently sample sizes are generally small and the experimental uncertainties in highly turbulent regions are large. Since the laser-Doppler anemometer is a non-interfering instrument that does not depend on the rheological or intensive properties of the working fluid, it perhaps provides the only technique which has the potential of yielding accurate results in a dilute polymer flow.

Rudd (1972), Logan (1972) and Kumor & Sylvester (1973) have made extensive laser anemometer measurements in drag-reducing flows. Rudd and Logan both used a 12·7 mm square duct for their measurements. The extensive laser anemometry survey of a square-duct water flow by Melling & Whitelaw (1973) clearly shows that the secondary corner flows affect the flow throughout the entire cross-section. In fact they concluded that it is very difficult, if not impossible, to achieve a reasonable degree of symmetry in square-duct flow. They also concluded that there is no location within a square duct where a single traverse is unaffected by the three-dimensional nature of the flow. Logan recognized the problem, measured the secondary flow and calculated that shearing velocity values based upon pressure drop were 30–40 % low compared with the two-dimensional values of shearing velocity. This ambiguity is evident in the abnormally high results for the normalized solvent turbulent intensities given by both Rudd and Logan. Despite a possible correction, the fact remains that a square-duct flow is a three-dimensional asymmetric flow and it is not apparent whether the polymer additive has affected the secondary flows, the turbulent processes or both. Kumor & Sylvester used a 203 mm square duct and made measurements in the boundary layer above a submerged off-centre flat plate. The secondary flows and pressure gradient in this configuration are not known, and no measurements of solvent velocity were offered. In summary, all of these experimental configurations have secondary flows and pressure gradients whose effects are difficult to understand. Consequently, the effect of the polymer additive on the turbulence is not clear.

The experimental results of this study differ significantly from the square-duct measurements mentioned above. Therefore the experimental apparatus, procedure and data reduction used here will be presented in some detail. The results will be compared with these previous measurements and then used to test other prediction techniques and hypotheses for drag reduction.

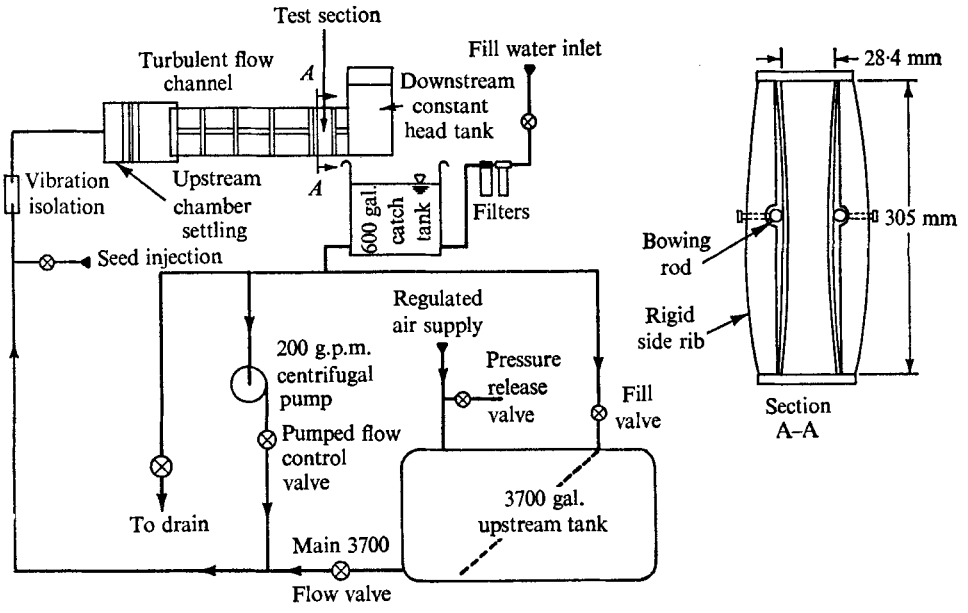

FIGURE 1. Schematic of flow channel and circulation system.

2. Experimental methods

2.1. *Water channel and flow system*

The experiments were conducted in the two-dimensional channel shown in figure 1. The channel is 305 mm tall and has a cross-sectional area of 0·83 m^2 and a hydraulic diameter of 50 mm. Its centre-line width of 26·02 mm was checked at various flow rates and found to be constant to within $\pm$ 0·03 mm. The unique feature of the channel is that the 6·4 mm thick Plexiglas side walls are uniformly bowed inwards by 1·19 mm along their entire length. This allows the spatial resolution of the laser anemometer to be maximized in the near-wall region. Various baffles in the upstream settling chamber redistribute the inlet pipe flow such that a uniform low-disturbance flow enters the channel. The channel is 1·78 m long, and the centre of the test section is 1·40 m downstream of the Borda-type entrance.

Fluid is forced through the channel either by a centrifugal pump or by pressurizing a 14·01 m^3 upstream fluid reservoir with air. The pump system, which recirculates fluid, was used when the laser anemometer was being set up and for the solvent (water) data runs. The pressurized flow mode, which is a 'once-through' system, was used when the working fluid was a dilute polymer solution, thereby minimizing polymer degradation. All piping, valves and fittings are either stainless steel, PVC or Plexiglas.

2.2. *Side-scatter laser-Doppler anemometer*

The basic function of the laser-Doppler anemometer is to measure the Doppler-shifted frequency of laser radiation scattered by small particles which are

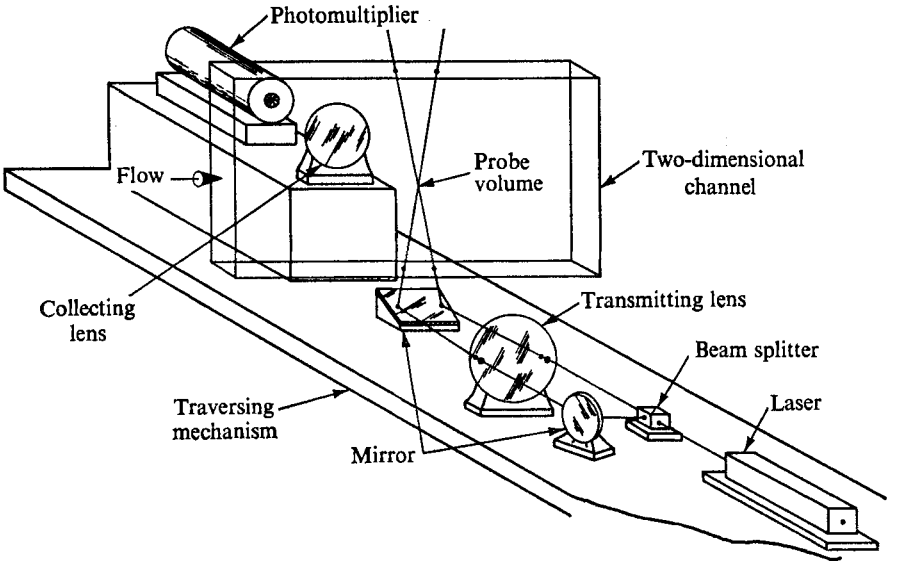

FIGURE 2. Side-scatter laser anemometer measuring individual realizations.

moving with the fluid. The Doppler frequency is directly proportional to a single component of the fluid velocity when the particles accurately follow the flow. In these experiments, the geometry of the anemometer was arranged such that the streamwise component of the velocity was measured. The laser-Doppler anemometer was of the individual-realization type, and measured the period of 10 cycles of a Doppler burst scattered from a single particle. The essential points about a laser anemometer measuring individual realizations are that the signal is not continuous and that velocity realizations occur only when a scattering centre is within the probe volume (see Donohue, McLaughlin & Tiederman 1972). The appearance of a scattering centre within the probe volume is a random event with a probability of occurrence in a certain time interval proportional to the volume of fluid swept through the probe volume during that time interval. An ensemble of individual realizations is used to form estimates of the mean velocity and the root mean square of the streamwise velocity fluctuations.

A schematic diagram of the basic optical set-up, which was a dual-scatter or fringe anemometer system, is shown in figure 2. The system used a 5 mW helium–neon laser and a RCA model 7326 photomultiplier. The beam splitter, mirrors and transmitting lens yielded two focused, temporally and spatially coherent, plane-polarized beams which were parallel to the side walls of the channel and intersected at the vertical centre of the flow channel. Figure 2 shows how the bowed walls and the laser optics were used to give the best possible spatial resolution – that is, the maximum dimension of the beam crossing was parallel to the wall and the smallest dimension normal to the wall.

The scattered light was collected from a cone whose axis was at an angle of 90° to the plane of the incident beams. This allowed the entire optical set-up to be mounted on a single, structurally sturdy base which contained a traversing

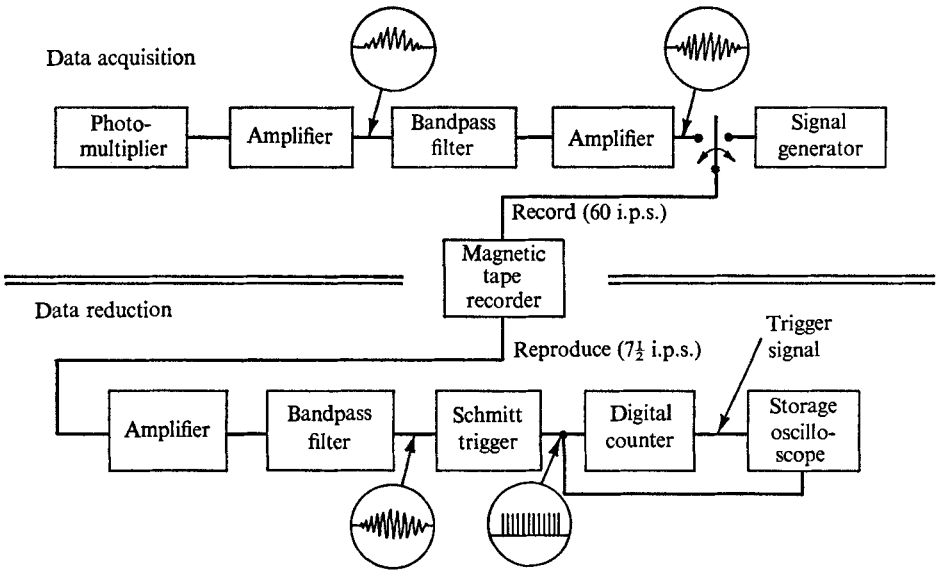

FIGURE 3. Block diagram of data acquisition and reduction system.

mechanism that allowed accurate ($\pm 0{\cdot}025$ mm) mechanical movement. The side-scatter arrangement also eliminated essentially all the optically generated noise from the photomultiplier tube's field of view and made it easy to reduce optically the long dimension of the probe volume.

In water the optics yielded a beam intersection angle θ of $5{\cdot}59°$. Thus, the Doppler frequency (per m/s) was 205·2 kHz and the interference-fringe spacing was 4·88 μm. The maximum number of cycles observed in a Doppler burst was 40. Using these 40 fringes to define an 'effective probe volume', the diameter of the probe volume became 0·195 mm. Owing to the collecting lens and aperture, the only focused light reaching the photomultiplier came from the central 0·64 mm of the beam intersection. Thus, the probe volume was a cylinder with a length of 0·64 mm and a diameter of 0·195 mm. The 'physical' location of the centre of the probe volume was determined by the traversing mechanism and by optically locating the wall with laser beams. This procedure for optically locating the wall was calibrated by comparing the channel width as measured by an inside micrometer with that measured by traversing the probe volume across the flow channel and visually noting its intersection with the wall. The comparison verified that the optical technique was as accurate as the micrometer measurement.

The purpose of the data-acquisition electronics shown in figure 3 was to condition and record the electrical signals that resulted from light scattered by individual particles in the flow. The signal output from the photomultiplier had two components: a *Doppler* portion, which had a constant period and a Gaussian envelope, and also a longer-period component, called the *pedestal*, which was proportional to the scattering particles' transit time through the probe volume. A bandpass filter removed the pedestal component from the composite signal, in addition to removing random noise outside the frequency

range of interest. The amplified and bandpass-filtered signal (as shown in figure 3) was recorded on magnetic tape by a double-bandwidth recorder. The signal generator shown was used to provide identification marks on the magnetic tape.

The data-reduction scheme measured, verified and recorded the Doppler period of the signal resulting from the passage of a particle through the probe volume. Verification of each individual realization was absolutely necessary because Doppler bursts frequently have single or multiple cycles either missing or suppressed. Visual verification of a Doppler burst was achieved by checking each individual realization whose Doppler period was counted to ensure that 10 consecutive Doppler cycles from a single realization were being counted. This was accomplished by allowing a Schmitt trigger output to simultaneously trigger a storage oscilloscope and a digital counter which was operating in the 'period times ten' mode. When the operator had visually verified that the pulse train from the Schmitt trigger had 10 consecutive pulses, generated by 10 Doppler cycles, the counter reading was recorded for later processing. Only pulse trains which represented valid individual realizations were recorded: the remainder were rejected.

2.3. *Data analysis*

The purpose of the data analysis was to yield the best estimates of the time-average mean velocity $\overline{U}$, where

$$\overline{U} = \frac{1}{T}\int_t^{t+T} U(t)\,dt, \tag{1}$$

and the root mean square u' of the streamwise velocity fluctuations, where

$$u'^2 = \frac{1}{T}\int_t^{t+T} (U(t)-\overline{U})^2\,dt. \tag{2}$$

There are two significant errors which can be made if these estimates are made directly from the ensemble of individual velocity realizations. The first, called statistical biasing, was analysed by McLaughlin & Tiederman (1973) for the present conditions, where on the average the scattering particles are distributed uniformly throughout the flow. This bias in the histogram of individual velocity realizations occurs because during a small interval of time the probability of detecting a particle is proportional to the volume of fluid swept through the probe volume during that time. Therefore over a long interval of time it is probable that more particles will be counted which are moving faster than the time-average velocity than particles which are moving slower. As a result the mean velocity $\overline{U}_B$ calculated from the ensemble of velocity realizations, where

$$\overline{U}_B = \frac{1}{N}\sum_{i=1}^{N} U_i, \tag{3}$$

will be larger than the time-average mean. However, as shown by McLaughlin & Tiederman (1973), an improved estimate of the time-average mean velocity can be made by weighting each velocity realization U_i with a function which is

inversely proportional to the volume flow through the probe volume at that instant. The proposed weighting function is $1/U_i$, thus the improved estimate is

$$\overline{U} = \frac{\sum_{i=1}^{N} U_i(1/U_i)}{\sum_{i=1}^{N} \frac{1}{U_i}} = \frac{N}{\sum_{i=1}^{N} \frac{1}{U_i}}. \tag{4}$$

Since individual realizations of the Doppler period τ_i were measured, it is convenient to rewrite (4) in terms of τ_i. The result is

$$\overline{U} = \left(\frac{\lambda N}{2 \sin \frac{1}{2}\theta}\right) \Big/ \sum_{i=1}^{N} \tau_i, \tag{5}$$

where λ is the wavelength of the laser light. All estimates of the time-average mean velocity were calculated using (5).

The effect of statistical biasing upon the mean velocity estimates is as high as 10 % in regions where the turbulence intensity is of the order of 30 %. However, since the biasing primarily shifts the histogram of individual realizations to higher values, good estimates of the root mean square of the velocity fluctuations can be made from the biased ensemble. Consequently, estimates of u' were calculated from

$$u'^2 = \frac{1}{N-1} \sum_{i=1}^{N} (U_i - \overline{U}_B)^2. \tag{6}$$

The second source of significant non-random error in the velocity measurements is use of a finite probe volume to make measurements in a large velocity gradient. This problem, which is most severe in the near-wall region of the channel, has been described for laser-Doppler anemometers operating in the continuous-wave mode by Edwards *et al.* (1971) and Goldstein & Adrian (1971). Karpuk (1974) has recently shown that for anemometers operating in the individual-realization mode the estimate of the mean velocity given by (5) is still correct for finite probe volumes if the velocity gradient is linear. The small dimension of the probe volume normal to the wall described earlier resulted in an essentially linear velocity profile within the probe volume at all y locations and consequently no correction was made to the mean velocity estimates.

Also, the error in the estimate of the turbulent intensity u' due to a finite probe volume within a velocity gradient is most pronounced in the near-wall region. Karpuk (1974) has proposed a correction and has successfully applied it to recent LAMIR measurements inside the viscous sublayer of a water channel flow. The correction lowered his estimates of u' of the order of 10–20 % for $y^+ < 5$ and then became negligible for locations outside the viscous sublayer. Karpuk's correction has not been applied to the data presented here. However, in a qualitative sense, one can say that the estimates of u' will be slightly high owing to the finite size of the probe volume and that the error will increase as the wall is approached.

A final aspect of the data analysis which was used in reducing the data is a biasing correction for the probability density function. McLaughlin & Tiederman

(1973) have shown that the corrected and biased probability density functions are related by

$$\beta(U) = (\overline{U}/U)\beta_B(U), \tag{7}$$

where $\beta(U)$ and $\beta_B(U)$ are corrected and biased values of the probability density function respectively. The LAMIR provides discrete data points and the probability density function can be approximated by bias-corrected histograms. Then (7) becomes

$$\beta(U_j) = (\overline{U}/U_j)\beta_B(U_j), \tag{8}$$

where the U_j are the velocity values at the centres of the intervals making up the histogram and $\beta(U_j)$ is the normalized level of the histogram in the jth interval.

In summary, the mean velocity data and the histograms presented herein have been corrected to remove the statistical biasing. The turbulent intensity data require essentially no correction for statistical biasing and remain uncorrected for the effects due to the finite extent of the probe volume in a velocity gradient.

2.4. *Solution preparation*

All the dilute polymer solutions were prepared in 600 gallon batches of prefiltered water into which a slurry of polymer and isopropyl alcohol was mixed. All solutions were gently stirred for approximately 1 h before being drained into the 3700 gallon upstream reservoir. When the upstream reservoir was filled with enough polymer solution for the experiment, the entire batch was allowed to hydrate for an additional 8–12 h. The resulting solutions were very homogeneous and since the solution made only one passage through the channel, the fluid properties at the test section were constant throughout each experiment. In addition this preparation technique yielded solutions of essentially equivalent viscometric and drag-reduction properties.

2.5. *Flow seeding*

Since the laser-Doppler anemometer measures the velocity of particles entrained in the flow, it is important to select scattering particles which follow the turbulent motions. It is equally important to select particles which will scatter enough light to yield a good Doppler signal-to-noise ratio at the output of the photomultiplier tube. Fortunately, 5–10 μm diameter sand particles classified from AC Fine Test Dust will both adequately follow the flow and yield good Doppler signals. In particular the results of Hjelmfelt & Mockros (1965) indicate that a 10 μm diameter sand particle will follow a 2500 Hz fluctuation with an amplitude ratio of 0·95. Most of the turbulent fluctuations in these low-speed water flows had frequencies below 250 Hz, and thus the seed particles did follow the flow.

The make-up water used in these experiments originally contained a wide dispersion of particulate sizes that naturally yielded a nearly continuous Doppler signal. This background seed was effectively eliminated for all the experiments by passing the make-up water through a 0·5 μm filter and by repeated flushing of the flow channel. When the fluid and system were clean

Run	Re	$\overline{U}_{av}$ (m/s)	u_τ (m/s)	T (°C)	Polymer characteristics: Name	Concentration (p.p.m. by weight)	D_R (%)
SOL-14	17700	0·322	0·0210	26	None	0	0·0
SOL-15	18500	0·322	0·0198	27·5	None	0	0·0
SOL-12	24700	0·444	0·0247	26	None	0	0·0
SOL-13	55200	1·021	0·0549	23–26	None	0	0·0
DPS-5	20196	0·378	0·0187	24	AP273	100	31·6
DPS-6	26373	0·493	0·0228	24	AP273	100	34·6
DPS-7	44516	0·816	0·0340	25	AP273	100	38·9
DPS-10	20582	0·366	0·0190	26·5	837A	100	24·0
DPS-11	37490	0·666	0·0293	27	837A	100	35·0
DPS-12	46037	0·818	0·0334	26·5	837A	100	40·7
DPS-9	52449	0·942	0·0396	26	WSR-301	100	35·3

TABLE 1. Summary of experimental scope

enough that essentially no seed particles could be sensed by the laser anemometer, then the polymer solutions were prepared and 1 mg/l of the 5–10 μm seed particles were added to the fluid. In this way, the flow seed was sufficiently dilute to yield Doppler signals from individual particles. As mentioned earlier, this means that the signal was discontinuous. Typically, there was a particle in the probe volume only 3 % or less of the total time.

2.6. *Polymer solution viscosity*

The assumption that the viscosity of a dilute polymer solution is constant – that is, independent of the shear rate – is a poor assumption for the high-molecular-weight polyacrylamides used here. Since the kinematic viscosity appears in the non-dimensional wall-layer variables, the local value of the kinematic viscosity must be used to calculate these variables accurately. Thus, the viscosity of the dilute polymer solutions was measured as a function of shear rate over the range 15–1000 s^{-1} with a Brookfield and a Fann–Couette type viscometer.

3. Results

Mean and fluctuating velocity measurements were made in both solvent and drag-reducing turbulent channel flows. The general characteristics of these flows are tabulated in table 1. The Reynolds number was calculated using the bulk average velocity $\overline{U}_{av}$, the hydraulic diameter of the channel and the kinematic viscosity of the solvent. The bulk average velocity was obtained by a graphical integration of the mean velocity profile. The percentage drag reduction D_R was calculated by comparing the wall shear stresses in a solvent and a drag-reducing flow at equal Reynolds number.

The LAMIR data from the solvent flows were taken in order to demonstrate

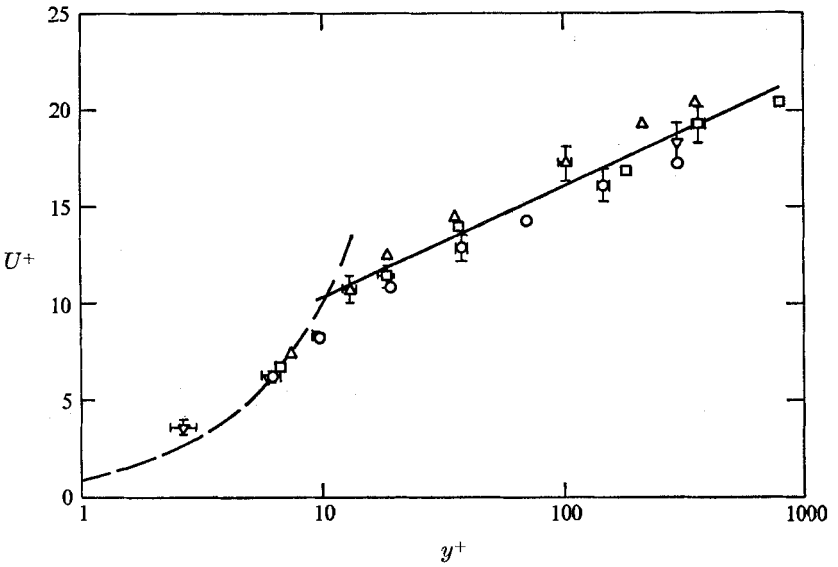

FIGURE 4. Solvent normalized mean velocity profiles. ○, Re = 17700; ▽, Re = 18500; △, Re = 24700; □, Re = 55200; ——, $U^+ = 5{\cdot}63 \log y^+ + 4{\cdot}69$; – – –, $U^+ = y^+$.

the standard characteristics of the flow facility and to illustrate the accuracy of the anemometer. Measurements were made at four Reynolds numbers Re: 17700, 18500, 24700 and 55200. The symmetrical nature of the flow adjacent to opposite walls of the channel was verified at Re = 24700, while measurements at locations 51 mm and 102 mm below the channel centre-line at two Reynolds numbers verified the two-dimensional nature of the flow. These results appear in Reischman (1973) and Tiederman, McLaughlin & Reischman (1973).

The mean velocity data for all solvent flows are shown in figure 4 in the non-dimensional wall-layer co-ordinates $U^+ = \overline{U}/u_\tau$ and $y^+ = yu_\tau/\nu$. $\overline{U}$ is the mean streamwise velocity; the wall shear velocity u_τ is defined as $(\tau_w/\rho)^{\frac{1}{2}}$; y is the co-ordinate normal to the wall; ρ is the fluid density and ν is the kinematic viscosity. The error bars in figure 4 and subsequent figures show the 95% confidence intervals for the reduced data.

The wall shear velocity u_τ used in figure 4 was computed from the slope of the velocity profile in the near-wall region. This computation was accomplished by using the equation

$$\tau_w = \mu(\partial\overline{U}/\partial y)_{y\simeq 0}, \tag{9}$$

velocity data from a y^+ value of approximately six and the fluid properties measured during the run. Here μ is the absolute viscosity. These estimates of u_τ were normalized and are compared with the pressure-drop data of Hussain & Reynolds (1970) in figure 5. It is important to note the good agreement. The polymer-solution data shown later will also rely upon this 'wall-slope' technique for deducing the shear stress at the wall.

The other important feature of figure 4 is the data at y^+ values greater than 30, which were used to determine the constant B in the equation

$$U^+ = 5{\cdot}63 \log y^+ + B. \tag{10}$$

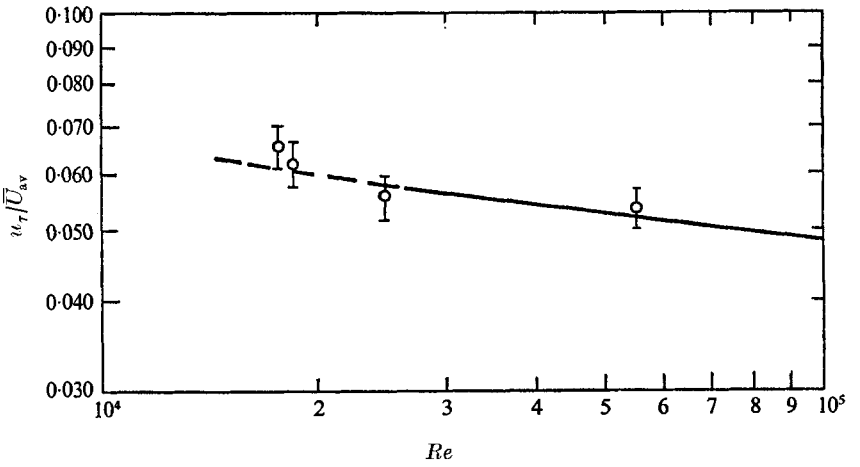

FIGURE 5. Shear-velocity correlation. ○, u_τ calculated from the slope of the near-wall velocity profile; ——, Hussain & Reynolds (1970).

Using the data for $y^+ > 30$ from all four runs and a least-squares regression, B was found to be 4·69 with a 5·4% uncertainty at the 95% confidence level. Although there is some evidence to indicate that both B and the von Kármán constant could be dependent upon Reynolds number (see Tennekes & Lumley 1972, p. 174; Patel & Head 1969), these data did not indicate any consistent variation with Reynolds number. Hence it was decided to specify the von Kármán constant and then to determine B from a least-squares regression of the data for all four Reynolds numbers. This value of B will be used later to determine the upward shift ΔB of the logarithmic portion of the velocity profile for the drag-reducing flows. It should also be noted that the value of 4·69 is within the range of values that other investigators have determined for B in similar flow situations (see Hussain & Reynolds 1970; Patel & Head 1969).

Figure 6 shows the variation in the root mean square of the streamwise velocity fluctuations for the four solvent flows as a function of y^+. The figure emphasizes the near-wall region of the flow. In general the data agree well with the hot-wire measurements of Hussain & Reynolds (1970) and Eckelmann & Reichardt (1971). The data do not agree so well with the solvent laser measurements of Rudd (1972). Undoubtedly the distinguishing feature of Rudd's measurements is that they were made in a square duct while the other three sets of measurements were made in two-dimensional channels with large aspect ratios.

Finally, with regard to both figures 4 and 6 an additional comment is needed about the measurements at $y^+ = 2{\cdot}5$. For these data the centre of the probe volume was only 0·109 mm from the wall. Since the probe volume was approximately 0·195 mm in diameter, its lower bound extended almost to the wall. Consequently the electronic filter setting which eliminated the pedestal frequencies from the Doppler bursts also filtered out some of the Doppler frequencies from slow moving particles passing through the lower portion of the probe volume (see Tiederman *et al.* 1973). As a result the measured mean velocity

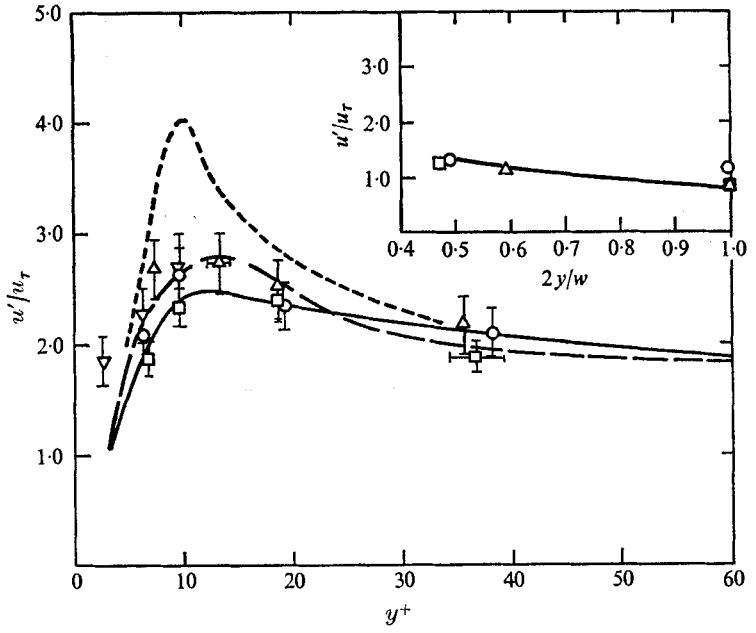

FIGURE 6. Solvent streamwise turbulent intensities. ○, Re = 17700; ▽, Re = 18500; △, Re = 24700; □, Re = 55200; – – –, Eckelmann & Reichardt (1971); ——, Hussain & Reynolds (1970); - - - - -, Rudd (1972).

was high. The fluctuation measurement was also high because there was a very large mean velocity gradient across the probe volume.

Velocity measurements were made in seven drag-reducing flows, whose general parameters are presented in table 1. Note that six of these runs were conducted with polyacrylamide polymers: three with Dow Chemical's Separan AP273, whose advertised weight-average molecular weight is $7{\cdot}5 \times 10^6$, and three with American Cyanamid's Magnifloc 837A, which has a weight-average molecular weight of 15×10^6. Polyox WSR-301 was used for the single experiment with polyethylene oxide. Union Carbide states that the weight-average molecular weight of WSR-301 is 4×10^6. For these seven experiments the solvent viscosity was used in calculating the Reynolds number. The shear velocity for the dilute polymer solutions was calculated from (9) using velocity data at $y^+ \approx 6$ and the absolute viscosity of the solution at the wall shear rate.

The mean velocity data are plotted in non-dimensional wall-layer co-ordinates in figures 7(*a*), (*b*) and (*c*). The results for each polymer species are shown in separate figures, where the profiles for the various levels of drag reduction are compared with the solvent profiles. In all cases, y^+ was calculated using a kinematic viscosity of the solution based upon the local shear rate. The logarithmic portions of the velocity profiles appear to be identical to the solvent data except for a vertical shift. This portion of the mean profile can be described by

$$U^+ = A \log y^+ + B + \Delta B. \tag{11}$$

For a given flow, ΔB is a constant, whose value is shown in figure 7. A buffer

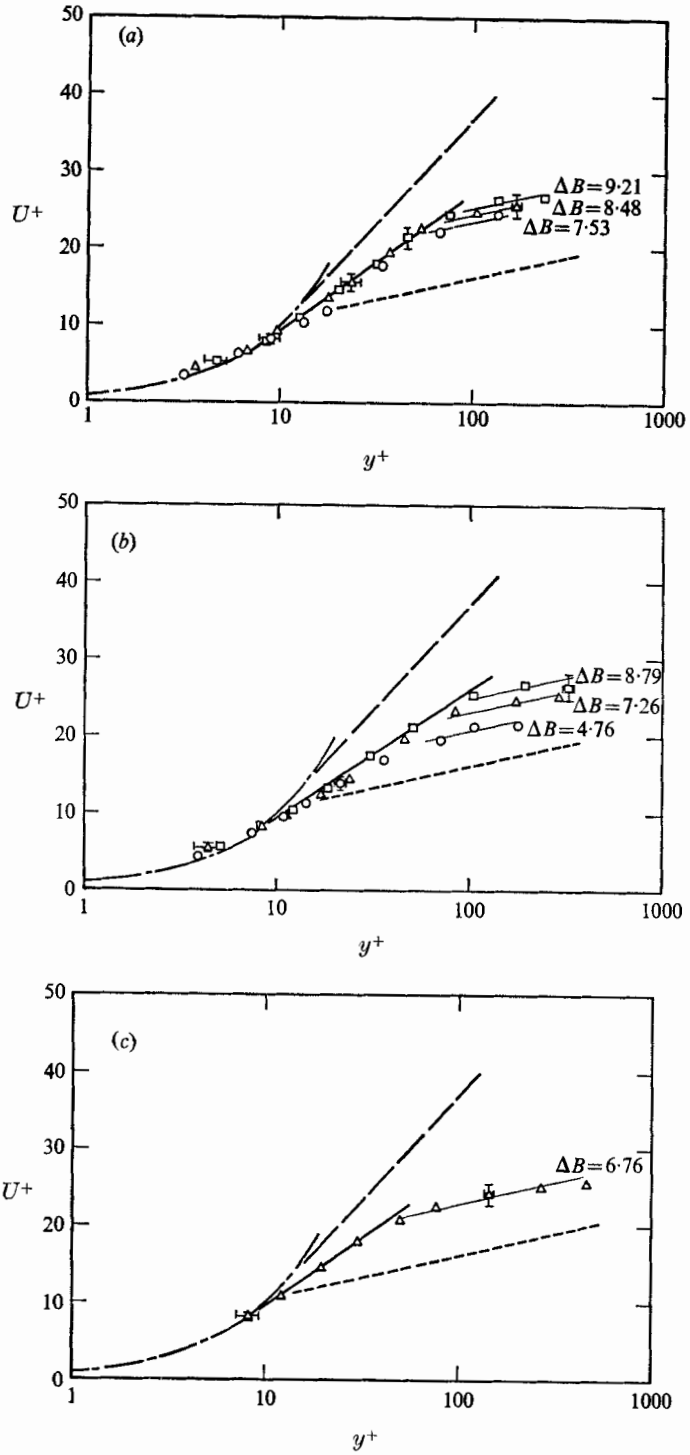

FIGURE 7. Mean velocity profiles for (*a*) Separan AP273, (*b*) Magnifloc 837A and (*c*) Polyox WSR-301. (*a*) ○, $Re = 20200$, $D_R = 31{\cdot}6\,\%$; △, $Re = 26400$, $D_R = 34{\cdot}6\,\%$; □, Re = 44500, $D_R = 38{\cdot}9\,\%$; ——, $U^+ = 17{\cdot}7 \log y^+ - 8{\cdot}2$. (*b*) ○, $Re = 20600$, $D_R = 24\,\%$; △, $Re = 37500$, $D_R = 35{\cdot}0\,\%$; □, $Re = 46000$, $D_R = 40{\cdot}7\,\%$; ——, $U_+ = 17{\cdot}7 \log y^+ - 7{\cdot}3$. (*c*) △, $Re = 52400$, $D_R = 35{\cdot}3\,\%$; ——, $U^+ = 17{\cdot}7 \log y^+ - 8{\cdot}0$. - - -, $U^+ = 5{\cdot}63 \log y^+ + 4{\cdot}69$; – – –, $U^+ = y^+$; – – –, ultimate profile of Virk *et al.* (1970).

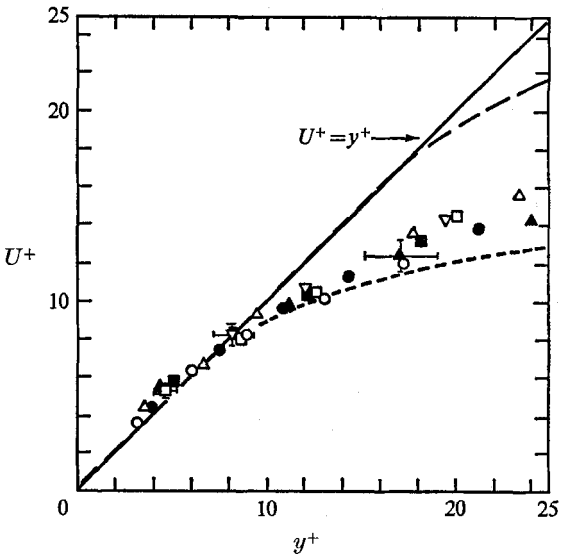

FIGURE 8. Normalized mean velocity profiles for drag-reducing solutions in the near-wall region. ○, AP273, Re = 20200; △, AP273, Re = 26400; □, AP273, Re = 44500; ▽, WSR-301, Re = 52400; ●, 837A, Re = 37500; ▲, 837A, Re = 37500; ■, 837A, Re = 46000; - - -, solvent; ——, $U^+ = y^+$; – –, Rudd (1972)

region exists between $y^+ \simeq 8$ and the beginning of the logarithmic region. The buffer-region data follow the curve

$$U^+ = C \log y^+ + D, \tag{12}$$

where C and D are given in figure 7. Also shown on figure 7 is Virk's 'ultimate profile' (see Virk *et al.* 1970). Clearly none of the seven flows substantiates the hypothesis that buffer-region data will follow Virk's ultimate profile for flows whose drag reductions are less than the maximum possible value.

All the velocity data in the near-wall region ($y < 25$) are shown again in figure 8 to illustrate clearly the extent of the viscous sublayer. The data for $y^+ < 8$ fit the curve $U^+ = y^+$ well. The most important aspect of the data is the departure of the mean velocity data from the linear curve for $y^+ > 8$–10. This result is in direct contrast to most previous data such as those of Rudd (1972), which are also shown in figure 8.

The intensities of the turbulent velocity fluctuations in the drag-reducing flows examined here are shown in figures 9 and 10 plotted in wall-layer coordinates. The present data are again compared with solvent channel data and the square-duct data of Rudd (1972). It can be seen that the present data differ significantly from those of Rudd. The distinct peak present in all the solvent data has disappeared and the higher values of u'/u_τ are distributed over a much wider range of y^+. There appears to be neither an extended linear curve up to a distinct peak nor a distinct peak in the turbulent intensities like those shown by Rudd (1972), Logan (1972) and Kumor & Sylvester (1973).

In the insets of figures 9 and 10, the root mean square of the streamwise fluctuations has been normalized with the local mean velocity and plotted as a

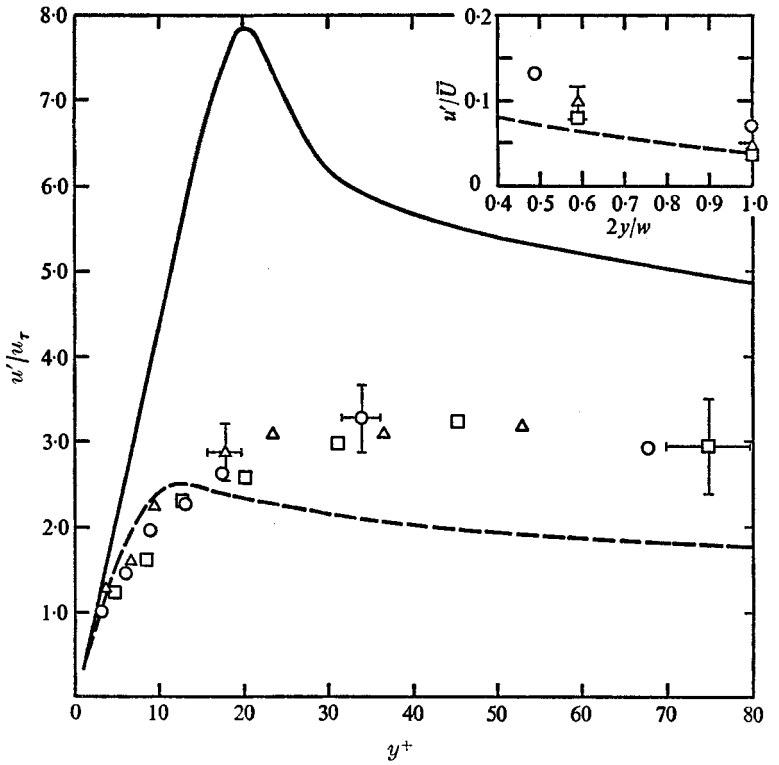

FIGURE 9. Drag-reducing turbulent intensities. Separan AP273: ○, Re = 20200; △, Re = 26400; □, Re = 44500. – –, solvent, Re = 41600; ——, polymer, Rudd (1972).

function of the physical distance normal to the wall. This representation emphasizes the outer portion of the flow. It is interesting to note that for $2y/w > 0{\cdot}4$ the Separan AP 273 data are above the solvent characteristic.

Another comparison between solvent and drag-reducing turbulent fluctuations is presented in figure 11. Here histograms of the individual realizations are compared for essentially constant values of y^+ and the Reynolds number. Note that for y^+ values near 10 both the mean and standard deviation of the drag-reducing flows are considerably lower than the comparable solvent values. However, at y^+ values near 20 and 30 there is not a significant difference between the solvent and drag-reducing histograms. Note also that both here and in figures 9 and 10 there is not much difference between the results for the solutions of the different polymers.

4. Discussion

The results presented here indicate that the modification of both the mean velocity profile and the streamwise turbulent intensity distribution when drag-reducing additives of high molecular weight are present is less than that previously reported by Rudd (1972), Logan (1972) and Kumor & Sylvester (1973). The differences are large enough that they can not be attributed to either ran-

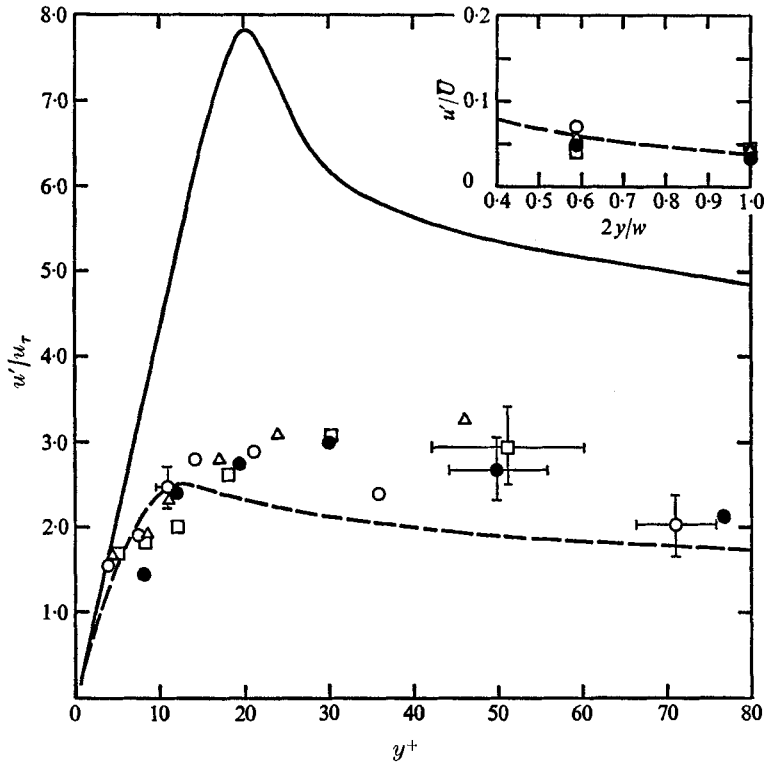

FIGURE 10. Drag-reducing turbulent intensities. Magnifloc 837A: ○, Re = 20600; △, Re = 37500; □, Re = 46000; ●, Polyox WSR-301, Re = 52400; – –, solvent, Re = 41600; ——, polymer, Rudd (1972).

dom experimental errors or to any other feature of the measurement and data-reduction techniques. This discussion will consider these differences, other hypotheses and models for predicting the upward shift of the logarithmic region.

The mean velocity measurements confirm the existence of three regions in a drag-reducing turbulent boundary layer, as shown in figure 7. A description of these three regions as indicated by the present data follows.

Viscous sublayer. The near-wall portion of the boundary layer is where viscous forces predominate and the velocity profile is linear. The non-dimensional velocity profile in this region is described by $U^+ = y^+$.

Logarithmic region. The velocity profile in the outer portion of the turbulent wall layer for drag-reducing two-dimensional channel flow fits the expression $U^+ = A \log y^+ + B + \Delta B$. The constants A and B are equivalent to those for a solvent flow, and ΔB is an additive constant. The mean velocity in this portion of the flow appears to be equivalent to a Newtonian flow and is apparently outside the major dynamic influence of the polymer additives.

Buffer region (elastic sublayer). The velocity in the region joining the viscous sublayer and the elevated logarithmic region is described by the expression $U^+ = C \log y^+ + D$. The empirical constants do not agree with Virk's 'ultimate

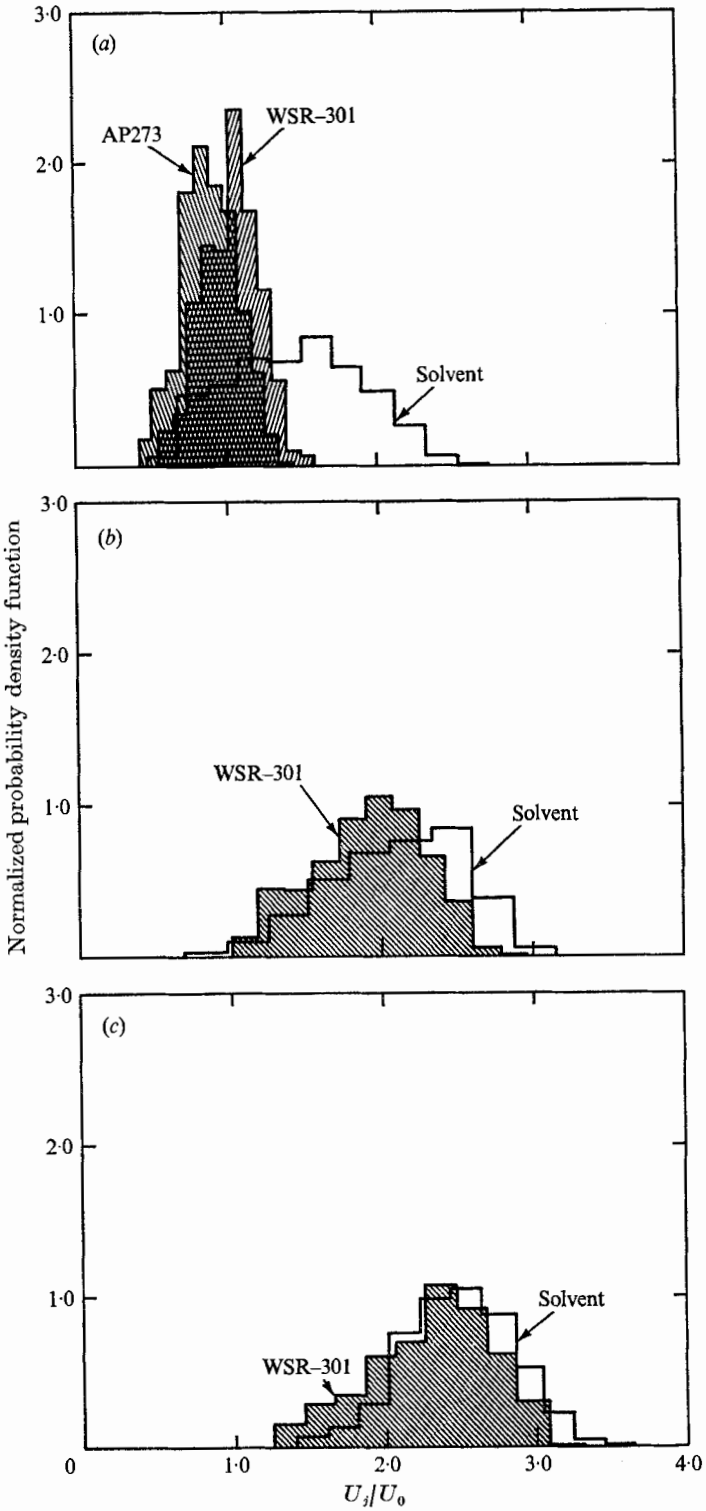

FIGURE 11. Comparisons of histograms. (*a*) Solvent: $Re = 55200$, $y^+ = 9{\cdot}6$, $N = 1001$. AP273: $Re = 44500$, $y^+ = 8{\cdot}6$, $N = 1001$. WSR-301: $Re = 52400$, $y^+ = 8{\cdot}2$, $N = 816$. (*b*) Solvent: $Re = 55200$, $y^+ = 18{\cdot}7$, $N = 1028$. WSR-301: $Re = 52400$, $y^+ = 19{\cdot}5$, $N = 1019$. (*c*) Solvent: $Re = 55200$, $y^+ = 36{\cdot}7$, $N = 1014$. WSR-301: $Re = 52400$,

profile'. However, this buffer region is the zone in which the effect of the polymer additives is seen most dramatically.

One of the most obvious features of the present mean velocity data is that they do not support the concept of a thickened viscous sublayer. As is shown quite clearly in figure 8, the linear portion of the velocity profile does not extend past a y^+ of about 9, and this is not significantly larger than the extent of the sublayer measured for the solvent flows. The important feature is not the absolute value of the non-dimensional thickness, but the fact that there was no detectable difference between the non-dimensional thicknesses for the solvent and the drag-reducing flows. This result is dramatically different from Rudd's (1972), in which the thickness of the viscous sublayer increased from $y^+ = 8$ for a solvent flow to $y^+ = 18$ for a drag-reducing flow. Logan's (1972) mean velocity measurements also showed an increase in the non-dimensional sublayer thickness, from a y^+ value of about 5 to $y^+ = 10$. Kumor & Sylvester's (1973) paper did not present solvent mean velocity data; but their drag-reducing flows had viscous sublayers as thick as $y^+ = 15$. However, it is highly unlikely that the flow was either two-dimensional in the case of Rudd and Logan or a constant-pressure-gradient two-dimensional boundary layer in the case of Kumor & Sylvester. In the fully developed two-dimensional channel flow of this present study, there was no indication of a thicker viscous sublayer accompanying drag reduction.

The effect of the three-dimensional flow field of a square duct upon the viscous sublayer is readily apparent in figure 6. Rudd's solvent measurements of u'/u_τ are considerably higher than our solvent measurements as well as hot-wire data from two other Newtonian two-dimensional channel flows. Logan's estimates of u'/u_τ for a water flow are even higher. Both Logan and Rudd deduced u_τ from pressure-drop measurements. As shown by Logan (1972), the local value of u_τ can be significantly larger than the average value of u_τ deduced from pressure-drop measurements even when the secondary flows in the square duct are small. Thus, Logan concluded that his estimates of u'/u_τ would be high because his estimate of u_τ was low. Recall that Melling & Whitelaw (1973) have also measured significant secondary flows in a square duct.

A further difference between the viscous sublayers of a drag-reducing square-duct flow and a drag-reducing two-dimensional channel flow is illustrated by the u'/u_τ measurements. As shown in figures 9 and 10, Rudd's values for a drag-reducing flow continue to increase linearly to a higher peak at $y^+ = 20$ than the present two-dimensional channel measurements. The peak in Rudd's drag-reducing measurements is higher than the peak in his solvent measurements, and it occurs at a larger value of y^+. Logan's measurements of u'/u_τ for a drag-reducing flow are similar to Rudd's, but the peak in u'/u_τ, which again occurs $y^+ = 20$, is only 6·0. The present measurements do not indicate a sharp peak; there is a broad plateau of maximum values over the range $20 < y^+ < 50$. It is believed that this difference, as well as the differences in the sublayer thickness, is due to the inherent three-dimensional nature of the square-duct apparatus used by the previous investigators. Consequently, it is hypothesized that the channel results presented here indicate how the polymer additive affects the

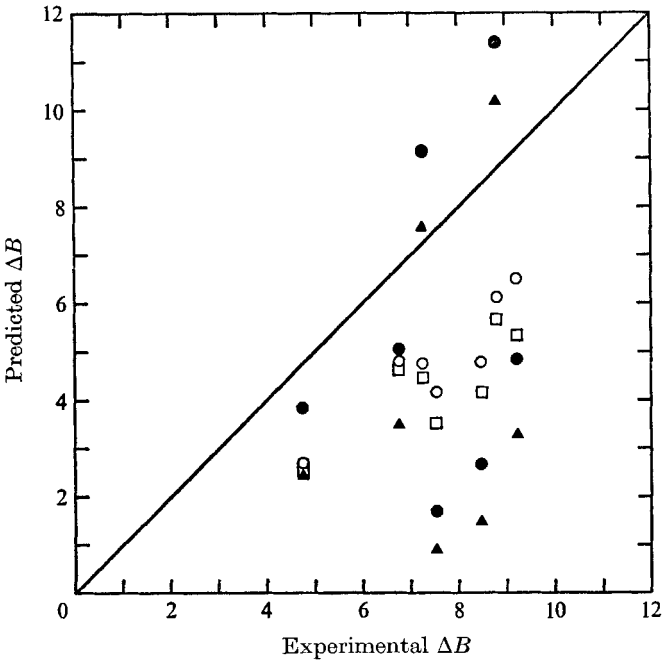

FIGURE 12. Comparison of experimental and predicted values of ΔB. ——, experimental ΔB = predicted ΔB; ○, Meyer (1966); □, Virk *et al.* (1970); ●, Rudd (1972); ▲, Seyer & Metzner (1969).

turbulent processes while the results of others also include an effect which the polymer additives have upon the secondary flows in a square duct.

Past efforts to measure turbulent velocities have been most successful in the logarithmic region of the mean velocity profile. Experimental results have usually shown a vertical displacement of the logarithmic portion of the universal velocity profile (ΔB shift) with no significant change in slope. Consequently, various techniques for predicting this ΔB shift have evolved. The present results provide a unique opportunity to test the universality of these various prediction schemes because both the polymer species and the polymer molecular weight as well as the flow conditions were varied in our test programme. Only those techniques which predict ΔB based upon information such as wall shear stress, average velocity, molecular weight of the polymer, polymer concentration, kinematic viscosity, intrinsic viscosity, solution temperature and channel dimensions were compared with the velocity data. To our knowledge there are currently five such techniques. They divide naturally into a group based upon Deborah numbers and a group based upon friction-factor information.

The methods proposed by Seyer & Metzner (1969), Elata, Lehrer & Kahanovitz (1966) and Rudd (1971) are all based upon a Deborah number (a ratio of the fluid's relaxation time and a characteristic time of the flow). Estimates of the fluid's relaxation time were made by using the first mode of Zimm's (1956) non-free draining model. The results of using the methods of Seyer & Metzner and

Rudd are compared with the experimental values of ΔB in figure 12. The agreement with the experimental results is poor. The ΔB shift predicted by the method of Elata *et al.* could be determined only to within a constant α and thus could not be shown on figure 12. However, the experimental values of α were not constant for any of the polymer species as required by the method.

This lack of agreement is not necessarily proof that the Deborah number is the wrong parameter because there are at least two possible reasons why the estimates of the fluid's relaxation time may be inaccurate. First, the estimates of the relaxation time were based upon the manufacturer's advertised weight-average molecular weight. The actual weight-average molecular weight will undoubtedly vary from batch to batch. More important, for these polymers there is a spectrum of molecular weights and it is likely that the weight average is not the molecular weight of the polymer molecules which are producing the drag reduction. Second, there is evidence (see Huang 1974) that sharp-edged entrances such as that used in our experiments will cause mechanical degradation and thereby lower the molecular weight of the effective polymer molecules in the channel. However, since it would be very difficult if not impossible to make a more accurate estimate of the relaxation time of the fluid in either these experiments or most applications, the poor agreement does show that the methods are not presently practical for engineering usage.

These experiments are a critical test of the prediction methods of Meyer (1966) and Virk *et al.* (1970) because they are both based upon flow conditions and friction-factor information. The results of these predictions are also compared with the experimental ΔB's in figure 12. The agreement between experiment and prediction is better for this group. There is less scatter and the trends are generally correct even though the magnitudes of the predictions are low. This result is not totally unexpected since the methods are basically an extrapolation from previous experiments.

Further attempts were made simply to correlate (not predict) ΔB using the fundamental wall-region time and length scales: the time between bursts $\overline{T}_B$ and the spacing λ of low-speed streaks (see Donohue, Tiederman & Reischman 1972). In particular the ratios $\nu/u_\tau^2\overline{T}_B$, $\nu/u_\tau^{*2}\overline{T}_B$ and $\lambda u_\tau/\nu$ were computed and plotted as functions of ΔB and the drag-reduction percentage. (The asterisk denotes the drag-reduction onset condition.) These quantities also failed to correlate the experimental values of ΔB. Thus, a universal prediction scheme based upon wall-layer quantities alone does not appear to be likely. It should be noted that all but one of the ΔB shifts were correlated to within the experimental error when the percentage drag reduction was used as the correlation parameter. Further experiments designed to verify the universality and possible engineering usage of such a correlation should be conducted.

The buffer region is obviously the region where the polymers have a strong influence on the mean velocity profile. In fact, figure 7 shows that the buffer region is the part of the mean velocity profile which becomes thicker, thereby shifting the logarithmic region upwards. As mentioned earlier, the hypothesized 'ultimate profile' of Virk *et al.* (1970) does not compare favourably with our data (see figure 7). The formulation of an alternative universal buffer-region profile

from our data is not justified at this time because the range of drag reductions was insufficient ($< 41\,\%$). However the slopes of the buffer-region velocity profiles agree to within $7\,\%$, which does suggest the possibility of a single constant for the slope of the mean profile in the buffer regime of these flows. Van Driest (1970) has proposed a similar constant, called the modified von Kármán constant, which is a function of polymer concentration. The existence of such a constant would no doubt lead to a careful reformation of classical mixing-length arguments as they apply to drag-reducing flows. However, our data are not sufficient to conclude that $C = 17{\cdot}7$ is a universal constant for the buffer-region profile. A series of experiments at higher levels of drag reduction is needed before such a conclusion would be justified.

The mean velocity measurements offer only implicit information concerning the structure of a turbulent flow. However, flow visualization can be employed to yield more explicit but less quantitative information about the flow processes. Obviously these two types of experiments should yield consistent information and indeed this is the case. For example the data from this study show a decrease in the intensity of the turbulent velocity fluctuations near the bounding surface when flows of equal Reynolds number are compared ($y^+ < 10$). The motion pictures of Donohue & Tiederman (1971) confirm these changes in the near-wall region of a drag-reducing flow. Dye injected at the wall showed a suppression of activity in the turbulent structure; that is, the dye was distributed much more evenly and the distinct features (such as low-speed streaks) became less identifiable and blended better into their surroundings. These observations are also consistent with the histograms of figure 11, where the decrease in the turbulent fluctuations near the wall is clearly visible.

Kline *et al.* (1967) have shown that the buffer region is a narrow region ($8 < y^+ < 30$) of intense turbulent action in a non-drag-reducing flow and subsequently Kim, Kline & Reynolds (1971) have shown that the greatest turbulent kinetic energy production occurs at $y^+ \approx 12$. The sharp maximum in the solvent turbulent intensity plot (u'/u_τ) occurs at the same y^+ location. Accordingly the buffer region is surmised to be intimately related to turbulent energy production. For a drag-reducing flow the peak which represents maximum energy production has moved away from the wall and has become much broader, which also implies buffer-layer thickening. Recall that the viscous sublayer was not thickened and the logarithmic region of the profile remained essentially the same in both the mean and fluctuating sense. It appears then that the alteration to the turbulent processes by polymer addition occurs in the productive, or buffer, region. This view is consistent with the results of Donohue, Tiederman & Reischman (1972), which showed that the addition of drag-reducing polymers directly affects the production of turbulence.

Lumley (1973) has recently presented a rather complete explanation of drag-reduction phenomena. However, several of his arguments have been developed to explain phenomena such as sublayer thickening which were not observed in this study. Consequently we conclude that the mechanism by which the polymer additives make their presence felt so strongly in the buffer region is still not thoroughly understood. It is clear, however, that the region of concern should

be the buffer region. The changes in turbulent production are being made in this region, and further probing should be concentrated there.

The authors gratefully acknowledge the support of the School of Mechanical and Aerospace Engineering at Oklahoma State University, and Professor D. K. McLaughlin for his helpful comments and criticisms. The manuscript was prepared while M.M.R. was a National Research Council Research Associate at the Naval Research Laboratory, Washington, D.C. Further acknowledgement goes to American Cyanamid, Inc., Dow Chemical Co. and Union Carbide for their generous donation of the drag-reducing additives.

REFERENCES

DONOHUE, G. L., MCLAUGHLIN, D. K. & TIEDERMAN, W. G. 1972 *Phys. Fluids*, **15**, 1970.

DONOHUE, G. L. & TIEDERMAN, W. G. 1971 The effect of a dilute, drag-reducing macromolecular solution on the viscous sublayer of a turbulent channel flow (16 mm motion picture). ASME/ESL Film Library, New York.

DONOHUE, G. L., TIEDERMAN, W. G. & REISCHMAN, M. M. 1972 *J. Fluid Mech.* **56**, 559.

ECKELMANN, H. & REICHARDT, H. 1971 *Proc. Turbulence in Liquids Symp., University of Missouri-Rolla* (ed. J. L. Zakin & G. K. Patterson), p. 144.

EDWARDS, R. V., ANGUS, J. C., FRENCH, M. J. & DUNNING, J. W. 1971 *J. Appl. Phys.* **42**, 837.

ELATA, C., LEHRER, J. & KAHANOVITZ, A. 1966 *Israel J. Tech.* **4**, 87.

GOLDSTEIN, R. J. & ADRIAN, R. J. 1971 *Rev. Sci. Instrum.* **42**, 1317.

HJELMFELT, A. T. & MOCKROS, L. F. 1965 *Appl. Sci. Res.* **18**, 149.

HOYT, J. W. 1972 *Trans. A.S.M.E., J. Basic Engng*, **94**, 258.

HUANG, T. T. 1974 *Phys. Fluids*, **17**, 298.

HUSSAIN, A. K. M. F. & REYNOLDS, W. C. 1970 *Stanford University Rep.* FM-6.

KARPUK, M. E. 1974 A laser-Doppler anemometer for viscous sublayer measurements. M.S. thesis, Oklahoma State University.

KIM, H. T., KLINE, S. J. & REYNOLDS, W. C. 1971 *J. Fluid Mech.* **50**, 133.

KLINE, S. J., REYNOLDS, W. C., SCHRAUB, F. A. & RUNSTADLER, P. W. 1967 *J. Fluid Mech.* **30**, 741.

KUMOR, S. M. & SYLVESTER, N. D. 1973 *A.I.Ch.E. Symp. Ser.* no. 130 (ed. N. D. Sylvester), vol. 69, p. 1.

LOGAN, S. E. 1972 Laser velocimeter measurement of Reynolds stress and turbulence in dilute polymer solutions. Ph.D. thesis, California Institute of Technology.

LUMLEY, J. L. 1969 *Ann. Rev. Fluid Mech.* **1**, 367–384.

LUMLEY, J. L. 1973 *J. Polymer Sci.: Macromol. Rev.* **7**, 263.

MCLAUGHLIN, D. K. & TIEDERMAN, W. G. 1973 *Phys. Fluids*, **16**, 2082.

MELLING, A. & WHITELAW, J. W. 1973 *Proc. Turbulence in Liquids Symp., University of Missouri-Rolla* (ed. J. L. Zakin & G. K. Patterson), p. 115.

MEYER, W. A. 1966 *A.I.Ch.E. J.* **12**, 522.

PATEL, V. C. & HEAD, M. R. 1969 *J. Fluid Mech.* **28**, 181.

REISCHMAN, M. M. 1973 Laser anemometer measurements in drag-reducing channel flows. Ph.D. thesis, Oklahoma State University.

RUDD, M. J. 1971 Drag reduction. *Ch.E. Prog. Symp. Ser.* no. 11, vol. 67 (ed. J. G. Savins & P. S. Virk), p. 21.

RUDD, M. J. 1972 *J. Fluid Mech.* **51**, 673.

SEYER, F. A. & METZNER, A. B. 1969 *A.I.Ch.E. J.* **15**, 427.

TENNEKES, H. & LUMLEY, J. L. 1972 *A First Course in Turbulence.* M.I.T. Press.

TIEDERMAN, W. G., MCLAUGHLIN, D. K. & REISCHMAN, M. M. 1973 *Proc. Turbulence in Liquids Symp., University of Missouri-Rolla* (ed. J. L. Zakin & G. K. Patterson), p. 172.

TOMITA, Y. 1970 *Bull. Japan Soc. Mech. Engrs*, **13**, 935.

VAN DRIEST, E. R. 1970 *J. Hydronautics*, **4**, 120.

VIRK, P. W. 1971 *J. Fluid Mech.* **45**, 417.

VIRK, P. W., MICKLEY, H. S. & SMITH, K. A. 1970 *Trans. A.S.M.E., J. Appl. Mech.* E **37**, 488.

ZIMM, B. H. 1956 *J. Chem. Phys.* **24**, 264.